MNRAS **000**, 1–10 (2016) Preprint 17 June 2016 Compiled using MNRAS LATEX style file v3.0

On the Astrid asteroid family

V. Carruba[1]⋆
[1] *UNESP, Univ. Estadual Paulista, Grupo de dinâmica Orbital e Planetologia, Guaratinguetá, SP, 12516-410, Brazil.*

arXiv:1606.05189v1 [astro-ph.EP] 16 Jun 2016

Accepted ... . Received 2016 ...; in original form 2016 May 02

ABSTRACT

Among asteroid families, the Astrid family is peculiar because of its unusual inclination distribution. Objects at $a \simeq 2.764$ au are quite dispersed in this orbital element, giving the family a "crab-like" appearance. Recent works showed that this feature is caused by the interaction of the family with the $s - s_C$ nodal secular resonance with Ceres, that spreads the inclination of asteroids near its separatrix. As a consequence, the currently observed distribution of the v_W component of terminal ejection velocities obtained from inverting Gauss equation is quite leptokurtic, since this parameter mostly depends on the asteroids inclination. The peculiar orbital configuration of the Astrid family can be used to set constraints on key parameters describing the strength of the Yarkovsky force, such as the bulk and surface density and the thermal conductivity of surface material. By simulating various fictitious families with different values of these parameters, and by demanding that the current value of the kurtosis of the distribution in v_W be reached over the estimated lifetime of the family, we obtained that the thermal conductivity of Astrid family members should be $\simeq 0.001$ W/m/K, and that the surface and bulk density should be higher than 1000 kg/m^3. Monte Carlo methods simulating Yarkovsky and stochastic YORP evolution of the Astrid family show its age to be $T = 140 \pm 30$ Myr old, in good agreement with estimates from other groups. Its terminal ejection velocity parameter is in the range $V_{EJ} = 5^{+17}_{-5}$ m/s. Values of V_{EJ} larger than 25 m/s are excluded from constraints from the current inclination distribution.

Key words: Minor planets, asteroids: general – minor planets, asteroids: individual: Astrid– celestial mechanics.

1 INTRODUCTION

The Astrid asteroid family is characterized by an unusual distribution in the $(a, \sin(i))$ plane, with a dispersion in inclination of its members at $a \simeq 2.764$ au much larger than that of members at other semi-major axis. Novakovic et al. (2016) recently showed that this feature of the Astrid family is caused by its interaction with the $s - s_C$ nodal secular resonance with Ceres. Asteroid crossing this resonance are significantly dispersed in inclination, causing the crab-like appearance of the family. The unusual distribution in inclination of the Astrid family also produces other consequences. Carruba & Nesvorný (2016) observed that the current distribution of the v_W component of terminal ejection velocities field computed from inverting Gauss equation for this family is characterized by a leptokurtic distribution, i.e., a distribution with larger tails and more peaked than a Gaussian. If we define as kurtosis the ratio of the fourth momenta of a distribution with respect to the fourth power of its standard deviation, that for a distribution of n random variable x_i is given by:

$$k = \frac{\frac{1}{n}\sum_{i=1}^{n}(x_i - < x >)^4}{(\frac{1}{n}\sum_{i=1}^{n}(x_i - < x >)^2)^2}, \quad (1)$$

where $< x >= \frac{1}{n}\sum_{i=1}^{n} x_i$ is the mean value of the distribution, then Pearson γ_2 kurtosis is equal to k-3. Gaussian distributions are characterized by values of γ_2 equal to 0. The value of the Pearson γ_2 parameter for the whole Astrid family is quite high, but is closer to mesokurtic values if asteroids in the resonant region are excluded.

In this work we investigate what information on key parameters describing the Yarkovsky effect, such as the thermal conductivity of material on the surface and the mass density, can be obtained by studying the orbital diffusion of fictitious members of several simulated Astrid families. By checking on what time-scales the current value of $\gamma_2(v_W)$ can be reached, and for what values of the parameters describing the Yarkovsky force, constraints on the allowed range of values of these parameters can be, in principle, obtained. The

⋆ E-mail: vcarruba@feg.unesp.br

© 2016 The Authors

independent constraints provided by secular dynamics (and from the current inclination distribution of Astrid members) could then be used to estimate the age of the Astrid family with a higher precision than that available for other families.

2 FAMILY IDENTIFICATION AND LOCAL DYNAMICS

As a first step in our analysis we selected the Astrid family, as identified in Nesvorný et al. (2015) using the Hierarchical Clustering Method (HCM, (Bendjoya & Zappalà 2002)) and a cutoff of 60 m/s. 489 members of the Astrid dynamical group were identified in that work. We also selected asteroids in the background of the family, defined as a box in the $(a, e, \sin(i))$ domain. We selected asteroids to within the minimum and maximum values of Astrid proper elements, plus or minus 0.02 au, 0.02, and 0.02 in proper a,e, and $\sin(i)$, respectively, with the exception of the maximum values in a that was given by the semi-major axis of the center of the 5J:-2A mean-motion resonance. 588 asteroids, 99 of which not members of the Astrid group, were identified in the background of the family so defined.

Fig. 1 displays the orbital location of family members (black full dots) and local background asteroids (black open dots) in the (a, e) (top panel) and $(a, \sin(i))$ (bottom panel) domains. The Astrid family numerically dominates the population in the local background: 83.1% of the asteroids in the region are members of the HCM family. One can also notice the spread in $\sin(i)$ of Astrid members at $a \simeq 2.765$ au, caused by the nodal linear secular resonance with Ceres $s - s_C$, as shown in Novakovic et al. (2016).

We then turned our attention to the physical properties of objects in the Astrid region. We checked which asteroids have information in the three major photometric/spectroscopic surveys (ECAS (Eight-Color Asteroid Analysis, Tholen et al. (1989)), SMASS (Small Main Belt Spectroscopic Survey, Bus & Binzel (2002a,b)), and S3OS2 (Small Solar System Objects Spectroscopic Survey, Lazzaro et al. (2004)), in the Sloan Digital Sky Survey-Moving Object Catalog data, fourth release (SDSS-MOC4 hereafter, Ivezić et al. (2001)), and in the WISE survey (Masiero et al. 2012). Taxonomic information was deduced for the SDSS-MOC4 objects using the method of DeMeo & Carry (2013). We obtained taxonomic information for 20 asteroids, while 207 bodies had values of geometric albedo in the WISE data-set. Fig. 2 displays our results for these objects. The Astrid family is a C-complex family, and C-complex objects dominate the local background: out of 207 bodies with information on geometric albedo, only 5 (2.4% of the total) have $p_V > 0.12$, and are possibly associated with a S-complex composition. No taxonomic or albedo interlopers were identified in the Astrid HCM group.

How much the local dynamics is responsible for the current shape of the Astrid family? To answer this question, we obtained dynamical maps in the domain of proper $(a, \sin(i))$ with the method described in Carruba (2010), based on the theory developed by Knežević and Milani (2000). We integrated 1550 particles over 20 Myr under the gravitation influence of i) all planets and ii) all planets plus Ceres as a massive body[1] with $SWIFT_MVSF$, the symplectic integrator based on $SWIFT_MVS$ from the *Swift* package of Levison and Duncan (1994), and modified by Brož (1999) to include on line filtering of osculating elements. The initial osculating elements of the particles went from 2.730 to 2.828 au in a and from 1.00° to 2.45° in i. We used 50 intervals in a and 31 in i. The other orbital elements of the test particles were set equal to those of Ceres at the modified Julian date of 57200.

Fig. 3 displays our results for the two maps. For the case without Ceres (panel A) the orbital region of the Astrid family is quite stable and regular, with most of the perturbations caused the 3J:-1S:-1A and 5J:-2A mean-motion resonances. More interesting is the case where Ceres was treated like a massive body (panel B). As observed by Novakovic et al. (2016), the linear nodal secular resonance $s - s_C$ now appears in the region. Objects whose pericenter frequency is within ±0.3 arc-sec/yr from $s_C = -59.17$ arc-sec/yr, likely resonators in the terminology of Carruba (2009), are shown as black full dots in this figure. Two other secular resonances involving the nodal frequency s_C of Ceres are also observed. Since the difference for the values of the g_5 and g_7 precession frequency of the pericenter of Jupiter and Uranus is small (4.257 and 3.093 arcsec/yr, respectively, which yield a difference of 1.164 arcsec/yr (Knežević and Milani 2000)), resonances of resonant argument involving $s - s_C$ and combinations of these two frequencies that satisfy the D'Alembert rules of permissible arguments are close in proper element space with respect to the main resonance $s - s_C$. In this work we called such resonances "harmonics" of the main resonance. We identified the $s - s_C - g_5 + g_7$ and $s - s_C - 2(g_5 + g_7)$ harmonics, whose likely resonators are shown in Fig. 3 as full squares and full hexagons, respectively.

To study the resonant dynamics of the Astrid family members, we integrated the 489 HCM Astrid asteroids with the same scheme used to obtain the dynamical map in Fig. 3, panel B. We then i) identify the likely resonators in the $s - s_C$ resonance, and studied the time evolution of the resonant argument $\Omega - \Omega_C$. We identified 96 likely resonators, and 19 objects (19.8% of the total) whose resonant argument librated around ±90° for 20 Myr, the length of the integration. Unfortunately, the limited number of objects in librating states of the $s - s_C$ resonance does not allow to use conserved quantities of this resonance to obtain information on the initial ejection velocity field, as done by Vokrouhlický et al. (2006b) for the Agnia family and the z_1 secular resonance, or, more recently, by Carruba et al. (2015b) for the Erigone family and the z_2 resonance. No asteroid was identified in librating states of the $s - s_C - g_5 + g_7$, $s - s_C - 2(g_5 + g_7)$, and $s - s_c + g_5 - 2g_6 + g_c$ resonances. We then computed proper values of the resonant frequency s, its amplitude $\sin(i/2)$, and its phase Ω for the 19 resonant objects and Ceres itself.

Fig. 4 displays an $(a, \sin(i))$ projection of the 489 HCM Astrid asteroids, with the likely resonators shown in the same symbol code as in Fig. 3 (panel A). Panel B show a projection in the $(\sin(i/2)\cos(\Omega - \Omega_C), \sin(i/2)\sin(\Omega - \Omega_C))$ of the 19 asteroids observed to be in librating states of the

[1] The mass of Ceres was assumed to be equal to $9.39 \cdot 10^{20}$ kg, as determined by the Dawn spacecraft (Russell et al. 2015).

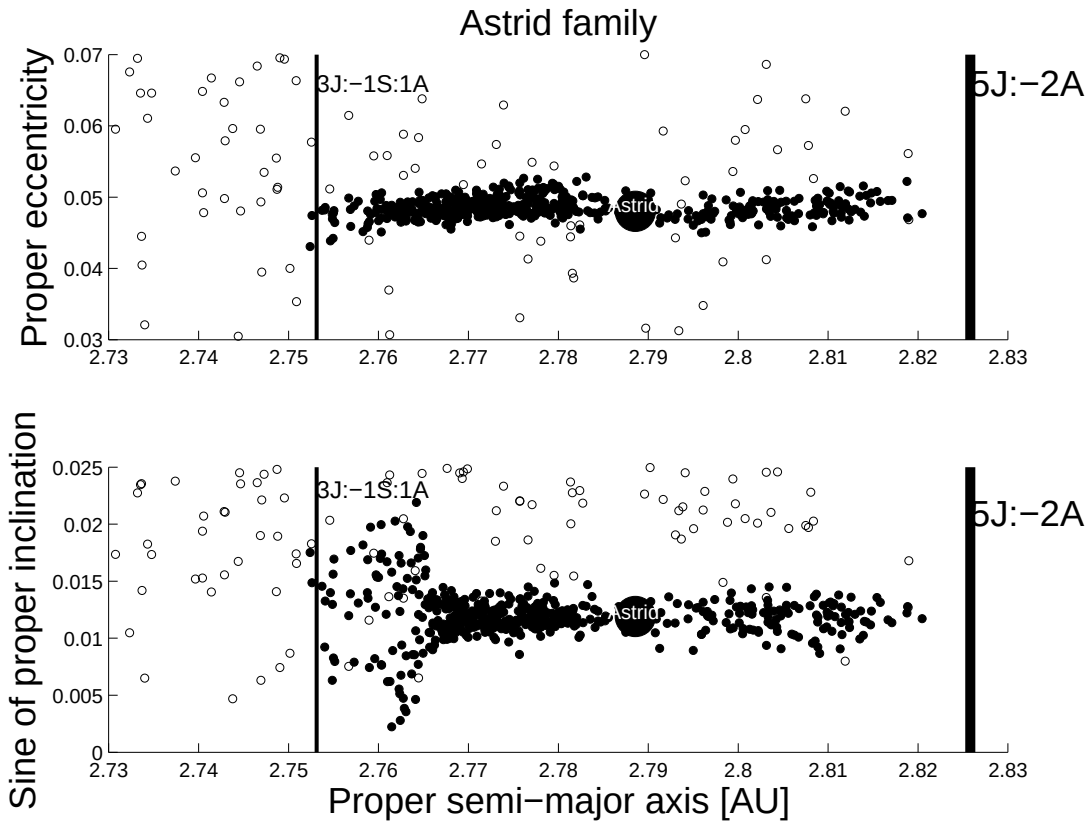

Figure 1. A (a, e) (top panel) and $(a, \sin(i)$ (bottom panel) projection of members of the HCM Astrid cluster (489 members, black full dots), and of the local background (588 members, black open dots). Vertical lines display the location of the local mean-motion resonances. The orbital location of 1128 Astrid is identified by a large black circle and it is labeled.

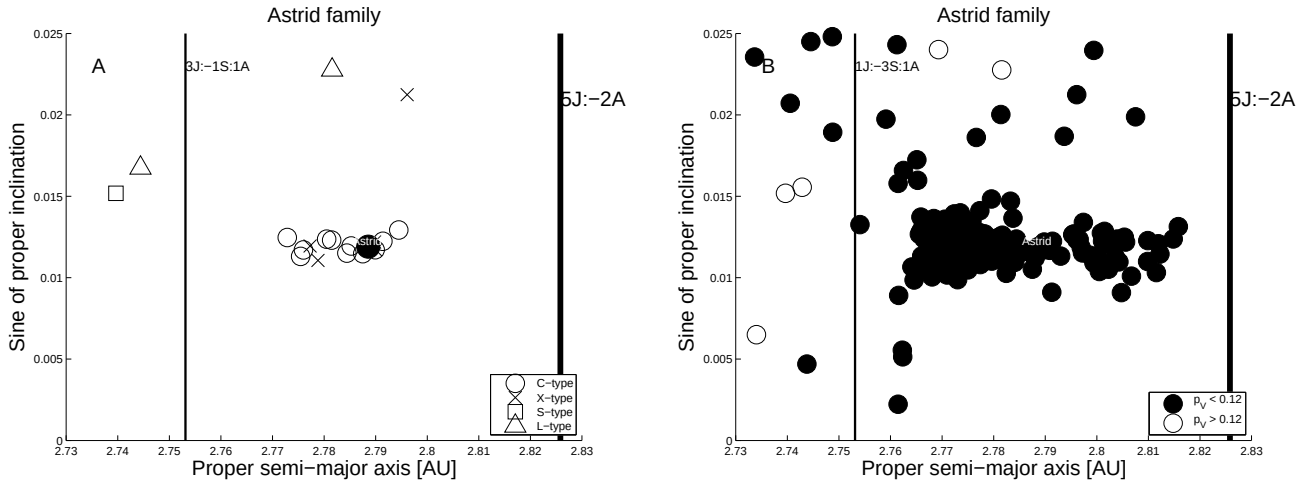

Figure 2. An $(a, \sin(i)$ projection of the 20 asteroids with taxonomic information (panel A) and of the 207 bodies with WISE albedo (panel B). See figures legends for the meaning of the used symbols.

$s - s_C$ resonance. One can notice that i), as observed from Novakovic et al. (2016), the spread in $\sin(i)$ of Astrid family members is indeed caused by the $s - s_C$ nodal resonance, and that, ii) resonant asteroids seems to oscillate around the stable point at $\Omega - \Omega_C = 0°$. No other stable point was identified in this work, and the width of the $s - s_C$ resonance is equal to 0.8 arcsec/yr.

To check how fast an initially tight cluster in the $(\sin(i/2)\cos(\Omega - \Omega_C), \sin(i/2)\sin(\Omega - \Omega_C)$ would be dispersed beyond recognition, so losing information about its initial configuration, we followed the approach of

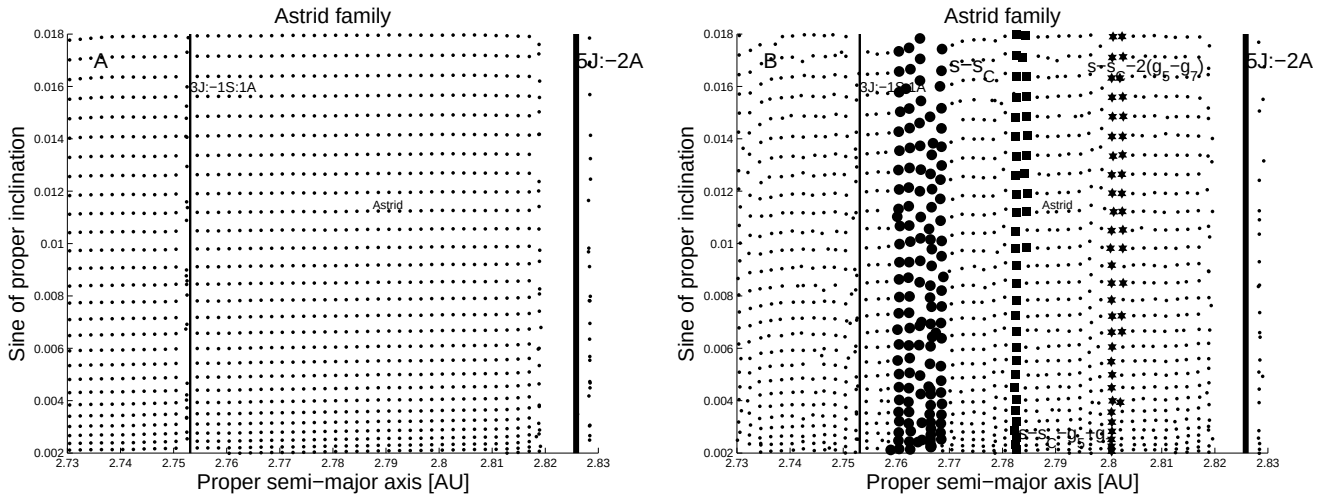

Figure 3. Dynamical maps for the orbital region of Astrid obtained by integrating test particles under the influence of all planets (panel A), and all planets and Ceres as a massive body (panel B). Unstable regions associated with mean-motion resonances appear as vertical strips. Secular resonance appear as inclined bands of aligned dots. Dynamically stable regions are shown as uniformly covered by black dots. Vertical lines display the location of the main mean-motion resonances in the area. Black filled dots in panel B show the locations of "likely resonators" in the $s - s_C$ secular resonance. Likely resonators in the $s - s_C - g_5 + g_7$ and $s - s_C - 2(g_5 + g_7)$ resonances are shown as full squares and full hexagons, respectively.

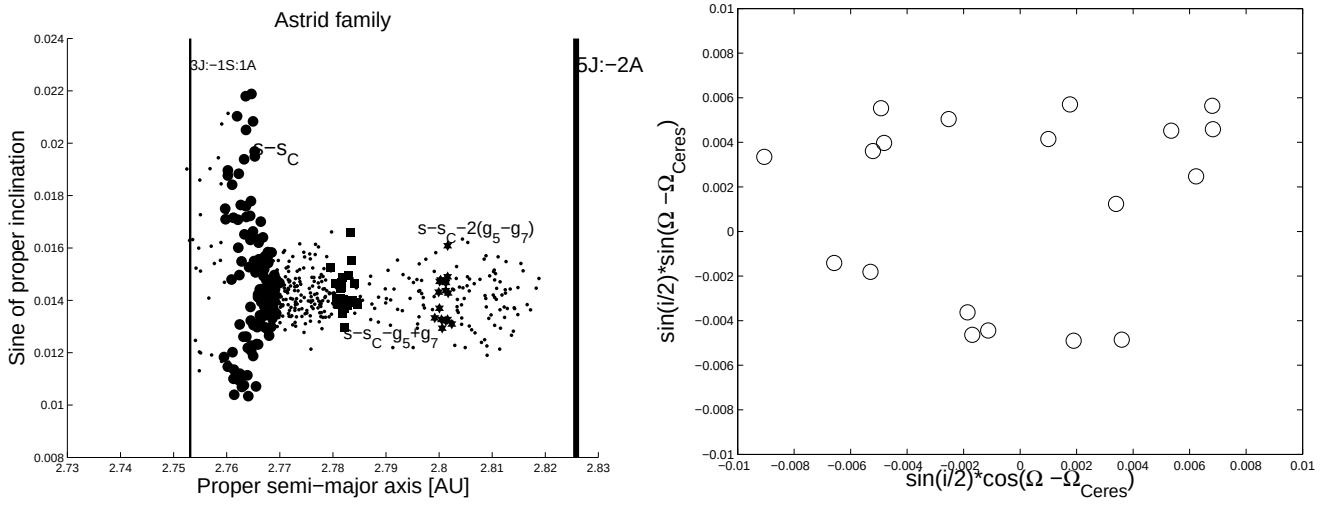

Figure 4. An $(a, \sin(i))$ projection of the 489 HCM Astrid asteroids, with the likely resonators shown in the same symbols code as in Fig. 3 (panel A). Panel B show a projection in the $(\sin(i/2)\cos(\Omega - \Omega_C), \sin(i/2)\sin(\Omega - \Omega_C)$ of the 19 asteroids observed to be in librating states of the $s - s_C$ resonance.

Vokrouhlický et al. (2006b). We generated 81 clones of 183405 2002 YE4, the lowest numbered object in a librating state of the $s - s_C$ resonance. The clones are in a 9 by 9 grid in eccentricity and inclination, with a step of 0.00001 in eccentricity and 0.0001 in inclination, and the elements of 183405 as central values of the grid. As observed for the z_2 resonant asteroids in the Erigone family (Carruba et al. (2015b), Fig. 9), the initially tight cluster becomes uniformly dispersed along the separatrix of the $s - s_C$ resonance. To quantify this effect, we used the polar angle Φ in the $(\sin(i/2)\cos(\Omega - \Omega_C), \sin(i/2)\sin(\Omega - \Omega_C)$ plane, as defined in Vokrouhlický et al. (2006b). At each step of the numerical simulation, we computed the dispersion D_Φ in the polar angle Φ defined as:

$$D_\Phi^2 = \frac{1}{N(N-1)} \sum_{i \neq j} (\Phi_i - \Phi_j)^2, \qquad (2)$$

where N = 81 is the number of integrated bodies and Φ_i is the polar angle of the i-th body (i = 1,...,N). Since we started with a compact cluster, D_Φ^2 is initially small ($\simeq 6.61°$), but grows with time because of the differential libration of the bodies in the resonance (Fig. 5). After only $\simeq$ 12 Myr, i.e., about two libration cycles of the $s - s_c$ resonance for 183405, the value of D_Φ^2 saturates at $\simeq 103°$, which corresponds to an uniform distribution of bodies along a circle Vokrouhlický et al. (2006b). This sets a lower limit on the timescale for dispersion of asteroids in the $(\sin(i/2)\cos(\Omega - \Omega_C), \sin(i/2)\sin(\Omega - \Omega_C)$ plane. Any

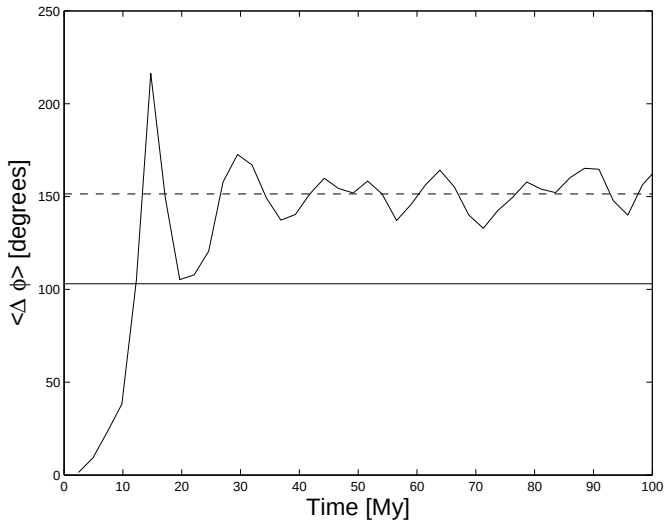

Figure 5. Temporal evolution of D^2_Φ of Eq. 2 for the 81 clones of 183405. The horizontal black line display the level corresponding to an uniform distribution of bodies along a circle Vokrouhlický et al. (2006b). The dotted line display the median value of D^2_Φ during the simulation.

family that reached this resonance more than $\simeq 12$ Myr ago, would have had its members completely dispersed along the separatrix of the $s-s_c$ resonance, which suggests that Astrid resonant members reached this resonance more than 12 Myr ago.

3 CONSTRAINTS ON TERMINAL EJECTION VELOCITIES FROM THE CURRENT INCLINATION DISTRIBUTION

The Astrid family is the product of a relatively recent collision: Nesvorný et al. (2015) estimate its age to be 140 ± 10 Myr, while Spoto et al. (2015), using a V-shape criteria, estimate the family to be 150 ± 32 Myr old. Monte Carlo methods (Milani & Farinella 1994; Vokrouhlický et al. 2006a,b,c) that simulates the evolution of the family caused by the Yarkovsky and YORP effects, where YORP stands for Yarkovsky-O'Keefe-Radzievskii-Paddack effect, could also be used to obtain estimates of the age and terminal ejection velocities of the family members (these models will be referred as "Yarko-Yorp" models hereafter). However, the age estimates from these methods depend on key parameters describing the strength of the Yarkovsky force, such as the thermal conductivity K and bulk and surface density ρ_{bulk} and ρ_{surf}, that are in many cases poorly known. Before attempting our own estimate of the family age and terminal ejection velocity field, here we analyze what constraints could be obtained on the possible values of terminal ejection velocities of the original Astrid family from its current inclination distribution.

In the Yarko-Yorp models, fictitious families are generated considering an isotropic velocity field[2], and assuming that the fragments are dispersed with a Gaussian distribution whose standard deviation follows the relationship:

$$V_{SD} = V_{EJ} \cdot (5km/D), \tag{3}$$

where V_{EJ} is the terminal ejection velocity parameter to be estimated, and D is the asteroid diameter. Nesvorný et al. (2015) estimated that the parent body of the Astrid family was 42.0 km in diameter, which yields an escape velocity of 33.0 m/s. Assuming that the V_{EJ} parameter of the terminal ejection velocity field would be in the range $0.2 < \beta < 1.5$, with $\beta = V_{EJ}/V_{esc}$, as observed for most families in the main belt (Carruba & Nesvorný 2016), then, expected values of V_{EJ} would be in the range from 5 to 50 m/s. If we only consider objects with $a > 2.77$ au, so as to eliminate the asteroids that interacted with the $s-s_C$ resonance, then the currently observed minimum and maximum values of $\sin(i)$ of family members are 0.0086 and 0.0148, respectively. Neglecting possible changes in $\sin(i)$ after the family formation, which is motivated by the fact that the local dynamics does not seems to particularly affect asteroids in this region (see Fig. 3), and will be further investigated later on, these values set constraints on the possible terminal ejection velocity parameter V_{EJ} with which the family was created. Currently, only 7 objects not members of the family are observed at sines of inclinations lower that 0.016, i.e., 1.5% of the current number of family members. We generated synthetic families for values of V_{EJ} from 5 m/s up to 40 m/s. Fig. 6 show an $(a, \sin(i)$ projection of the initial orbital dispersion of the members of the family generated for $V_{EJ} = 25$ m/s (panel A) and $V_{EJ} = 40$ m/s.

For $V_{EJ} = 25$ m/s 7 particles (1.5% of the total) had values of $\sin(i)$ outside the range of values currently observed, while for $V_{EJ} = 40$ m/s these number was 55 (11.5% of the total). Based on these considerations, it seems unlikely that the ejection velocity parameter V_{EJ} was larger than 25 m/s, or a larger number of asteroids outside the Astrid family at $a > 2.77$ au would be visible today. This implies that $\beta = \frac{V_{EJ}}{V_{esc}}$ was at most 0.76, excluding larger values associated with more catastrophic events.

4 EJECTION VELOCITIES EVOLUTION

Carruba & Nesvorný (2016) recently investigated the shape of the current distribution of the v_W component of terminal ejection velocity fields and argued that families that were produced with a V_{EJ} parameter smaller than the escape velocity from the parent body, are relatively young, and are located in dynamically less active regions, as is the case of the Astrid family, should be characterized by a leptokurtic distribution of the v_W component. This because, assuming that initial ejection velocities followed a Gaussian distribution, fragments with initial ejection velocities less than the escape velocity from the parent body would not be able to escape. This would produce a distribution of ejection velocities more peaked and with larger tails than a Gaussian one,

[2] Not all ejection velocities field are isotropic. If the fragmentation was not completely catastrophic, terminal velocities could be rather anisotropic. This could actually be the case for the Astrid family, as also discussed later in this paper. However, since in this section we are just interested in setting constraints to the maximum magnitude of the possible ejection velocity field, we prefer for this purpose to use a simpler approach.

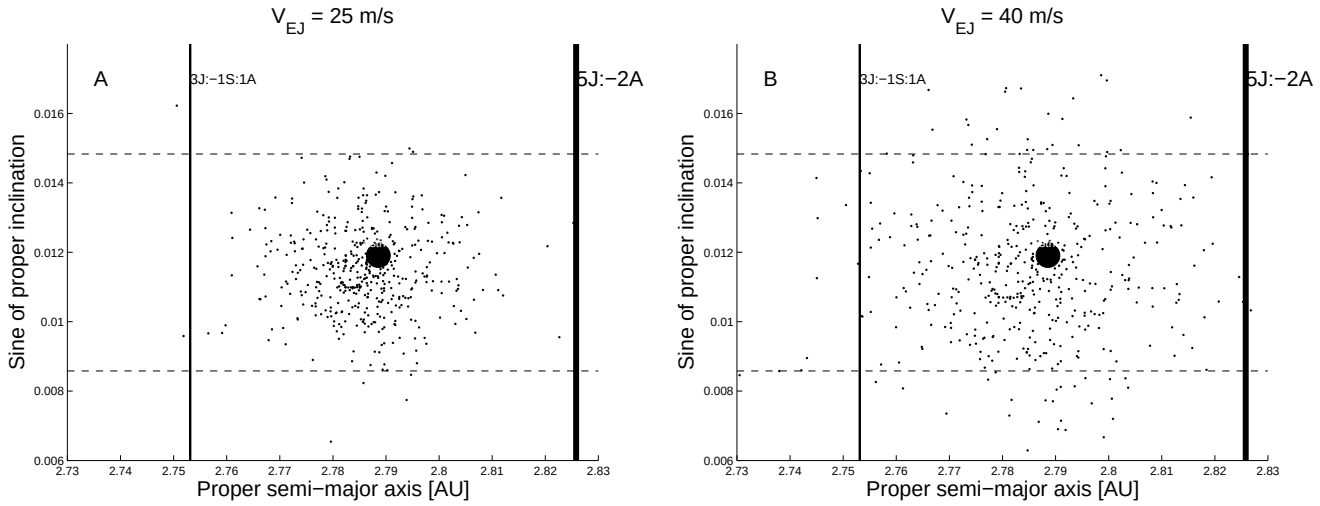

Figure 6. An $(a, \sin(i))$ projection of the initial orbital dispersion of a family generated with $V_{EJ} = 25$ m/s (panel A) and $V_{EJ} = 40$ m/s (panel B). The full black circle identifies the location of 1128 Astrid (that essentially corresponds with the family barycenter), while the dashed lines show the minimum and maximum values of $\sin(i)$ currently observed for members of the Astrid family with $a > 2.77$ au, i.e., those that did not yet interacted with the $s - s_C$ secular resonance. The other symbols have the same meaning as in Fig. 1.

i.e., leptokurtic. While the subsequent dynamical evolution would tend to cause the distribution of ejection velocities to be more mesokurtic, this effect would be less intense for families such Astrid, that are both relatively young and in dynamically less active regions.

One would therefore expect Astrid to be a relatively leptokurtic family. However, as also noticed in Carruba & Nesvorný (2016), the effect of the $s - s_C$ secular resonance tend to increase the dispersion in inclination values of the family members, and therefore of v_W. While the current value of γ_2, the parameter associated with the kurtosis of the v_W distribution (equal to 0 for mesokurtic or Gaussian distributions) of the whole Astrid family is quite large, ($\gamma_2 = 4.43$), if we only consider objects with $a > 2.77$ au that did not interacted with the secular resonance, the value of γ_2 is just 0.39, more compatible with a relatively somewhat leptokurtic family. This shows that most of the leptokurtic shape of the currently observed Astrid family is therefore caused by the interaction of its members with the $s - s_C$ secular resonance.

To investigate what information the v_W component of the terminal ejection velocities could provide on the initial values of the V_{EJ} parameter, we simulated fictitious Astrid families with the currently observed size-frequency distribution, values of the parameters affecting the strength of the Yarkovsky force typical of C-type asteroids according to Brož et al. (2013), i.e., bulk and surface density equal to $\rho_{bulk} = \rho_{surf} = 1300$ kg/m^3, thermal conductivity $K = 0.01$ W/m/K, thermal capacity equal to $C_{th} = 680$ J/kg/K, Bond albedo $A_{Bond} = 0.02$ and infrared emissivity $\epsilon = 0.9$. We also generated fictitious families with $V_{EJ} = 5, 10, 15, 20,$ and 25 m/s, the most likely values of this parameter, according to the analysis of the previous section. Particles were integrated with $SWIFT_RMVSY$, the symplectic integrator developed by Brož (1999) that simulates the diurnal and seasonal versions of the Yarkovsky effect, over 300 Myr and the gravitational influence of all planets plus Ceres. Values of v_W were then obtained by inverting the third Gauss equation Murray and Dermott (1999):

$$\delta i = \frac{(1-e^2)^{1/2}}{na} \frac{cos(\omega + f)}{1 + ecos(f)} \delta v_W. \quad (4)$$

where $\delta i = i - i_{ref}$, with i_{ref} the inclination of the barycenter of the family, and f and $\omega + f$ assumed equal to 30° and 50.5°, respectively. Results from Carruba & Nesvorný (2016) show that the shape of the v_W distribution is not strongly dependent on the values of f and $\omega + f$.

Fig. 7 displays the time evolution of the γ_2 parameter of the v_W distribution for the fictitious family with $V_{EJ} = 5$ m/s (panel A) and 10 m/s (panel B). The peak in the γ_2 value occurs when most particles interacted with the $s - s_C$ secular resonance and had their inclination value increased by this resonance. The current value of γ_2 of the Astrid family is not reached for any time inside the range of possible ages, as estimated by Spoto et al. (2015) (vertical red lines, the largest range of uncertainty for the age of this family in the literature. This range of ages corresponds to a 1-standard deviation confidence level, obtained by computing a Yarkovsky calibration, with 20% relative uncertainty, and with an assumed density of 1410 kg/m^3), neither for the simulations with $V_{EJ} = 5$ m/s nor that with $V_{EJ} = 10$ m/s. The situation is even worse for families with larger values of the ejection parameter, for which the peak in γ_2 is achieved earlier. This suggests that standard parameters describing the Yarkovsky force may not apply for the Astrid family.

Masiero et al. (2012) analyzed the effect that changing the values of the Yarkovsky parameters had on estimate of the family age, and found that the largest effect was associated with changes in the values of the thermal conductivity and bulk and surface density of asteroids, in that order. Based on these results, we first considered two other possible values of K, 0.001 and 0.100 W/m/k, and repeated our simulations for $V_{EJ} = 10$ m/s. Results are shown in Fig. 8.

In both cases, the current value of γ_2 is indeed achieved

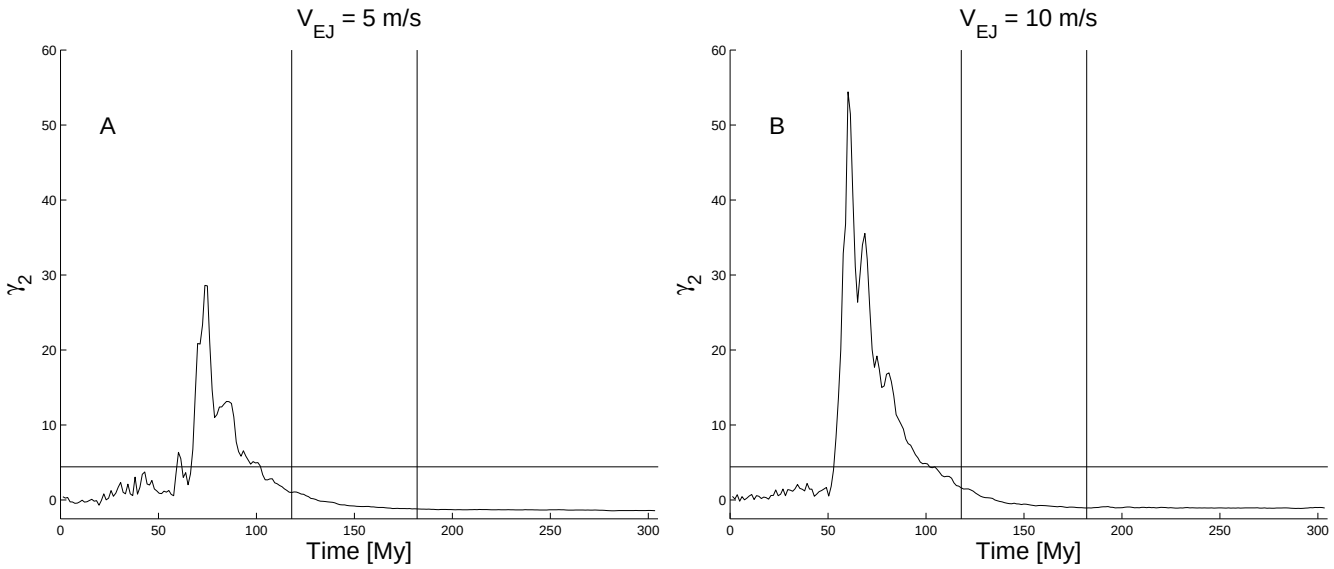

Figure 7. Time evolution of the Kurtosis parameter γ_2 for members of a fictitious family with V_{EJ} = 5 m/s (panel A) and 10 m/s (panel B). The horizontal black line displays the current value of γ_2 for the real whole Astrid family. The vertical lines identify the range of possible ages for the Astrid family, according to Spoto et al. (2015).

in the interval covering the uncertainty associated with Astrid age. In the second case, however, the fraction of objects with semi-major axis lower than 2.7646 au, that crossed the $s - s_c$ resonance, was too small at t = 182 Myr (the maximum possible age for Astrid), when compared with the current value (15.8%). This suggests that K = 0.001 W/m/K could be closer to the actual value of thermal conductivity of the real Astrid asteroids. We then considered the effect of changing the bulk and surface density, assumed equal, for simplicity. We used for the two sets of simulations $\rho_{bulk} = \rho_{surf}$ = 900 kg/m^3 and $\rho_{bulk} = \rho_{surf}$ = 1700 kg/m^3, that are at the extreme of the range of values for the density of C-type asteroids (DeMeo & Carry 2013). The other parameters were equal to previous values, and K = 0.001 W/m/K. Fig. 8, panels C and D, displays our results. While the values of γ_2 for the first simulation, do not reach the current value in the time interval covering the uncertainty associated with Astrid age, larger values of the density could be still compatible with our γ_2 test. Overall, our results suggest that the thermal conductivity K of Astrid members should be of the order of K = 0.001 W/m/K, while the mean density of Astrid fragments should be higher than 1000 kg/m^3. Remarkably, results obtained with the $\gamma_2(V_W)$ method are in good agreement with those obtained from independent methods (Spoto et al. 2015).

5 CHRONOLOGY OF THE ASTRID FAMILY

Now that the analysis of the current inclination distribution and our γ_2 test provided independent constraint on the values of the V_{EJ} parameter and of the thermal conductivity and density of Astrid members, we can try to obtain an independent age estimate for this family. We use the approach described in Carruba et al. (2015a) that employs a Monte Carlo method (Milani & Farinella 1994; Vokrouhlický et al. 2006a,b,c) to estimate the age and terminal ejection velocities of the family members. More details on the method can be found in Carruba et al. (2015a). Essentially, the semi-major axis distribution of simulated asteroid families is evolved under the influence of the Yarkovsky effect (both diurnal and seasonal version), the stochastic YORP force, and changes in values of the past solar luminosity. Distributions of a C-target function are then obtained through the equation:

$$0.2H = log_{10}(\Delta a/C), \tag{5}$$

where H is the asteroid absolute magnitude, and $\Delta a = a - a_{center}$ is the distance of each asteroid from its family center, here defined as the family center of mass. For the Astrid family this is essentially equal to the semi-major axis of 1128 Astrid itself. We can then compare the simulated C-distributions to the observed one by finding the minimum of a χ^2-like function:

$$\psi_{\Delta C} = \sum_{\Delta C} \frac{[N(C) - N_{obs}(C)]^2}{N_{obs}(C)}, \tag{6}$$

where $N(C)$ is the number of simulated objects in the $i-th$ C interval, and $N_{obs}(C)$ is the observed number in the same interval. Good values of the $\psi_{\Delta C}$ function are close to the number of the degrees of freedom of the χ^2-like variable. This is given by the number of intervals in the C minus the number of parameters estimated from the distribution (in our case, the the family age and V_{EJ} parameter). Using only intervals with more than 10 asteroids, to avoid the problems associated with small divisors in Eq. 6, we have in our case 7 intervals for $C < 0$ (see Fig. 9, panel A) and 2 estimated parameters, and, therefore, 5 degrees of freedom. If we assume that the $\psi_{\Delta C}$ probability distribution follows a law given by an incomplete gamma function of arguments $\psi_{\Delta C}$ and the number of degrees of freedom, the value of $\psi_{\Delta C}$ associated with a 1-sigma probability (or 68.23%) of the simulated

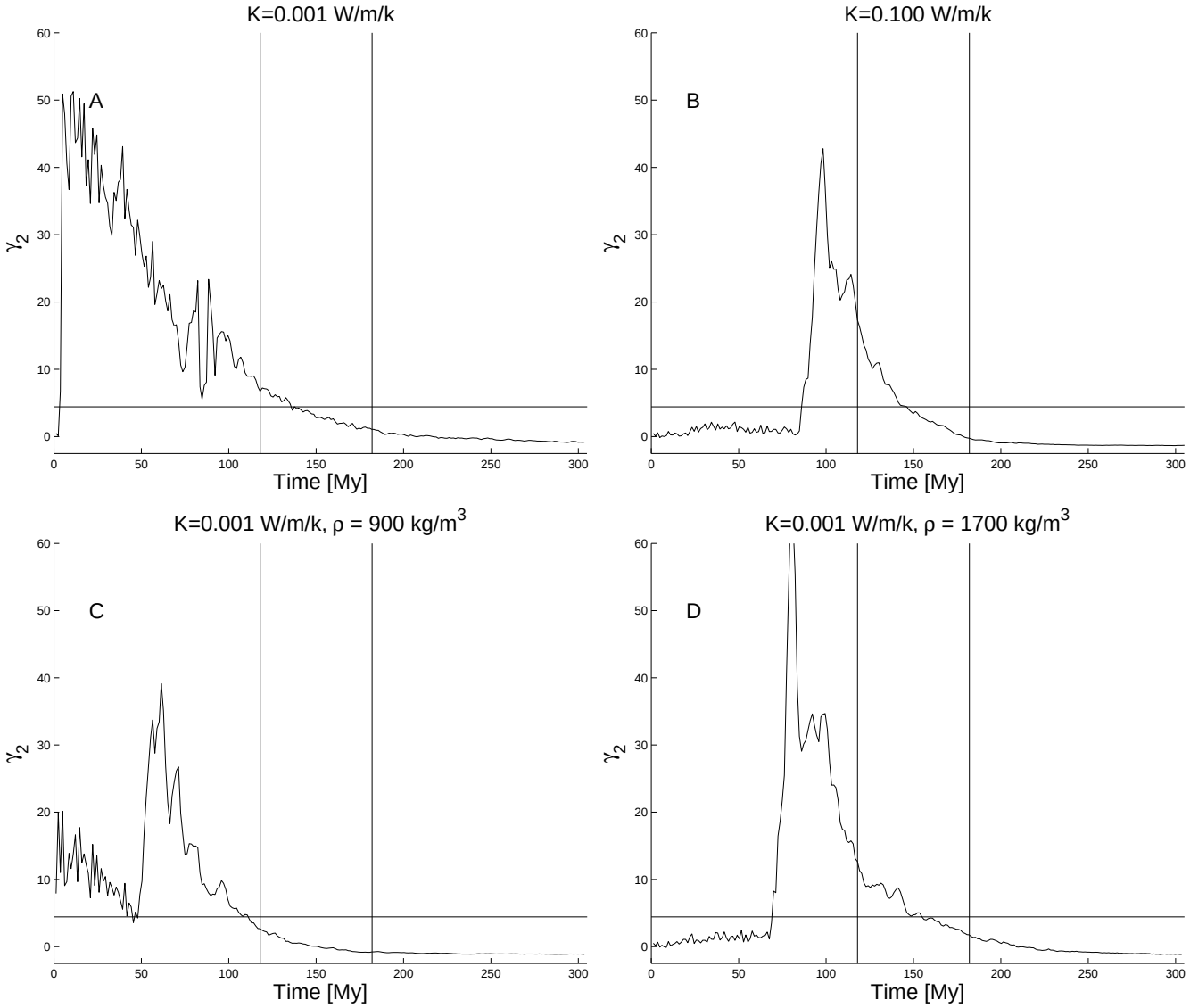

Figure 8. Time evolution of the Kurtosis parameter γ_2 for members of a fictitious family with $V_{EJ} = 10$ m/s and thermal conductivity $K = 0.001$ W/m/K (panel A) and 0.100 W/m/k (panel B). In panel C and D we display results for $K = 0.001$ W/m/K and $\rho_{bulk} = \rho_{surf} = 900$ kg/m^3, and $\rho_{bulk} = \rho_{surf} = 1700$ kg/m^3, respectively. The symbols have the same meaning as in Fig. 7.

and real distributions being compatible is equal $\psi_{\Delta C} = 4.3$ (Press et al. 2001).

The reason why we only considered negative values of C for our analysis is that the semi-major axis distribution (and, therefore, the C one) is quite asymmetric. 72.4% of family members are encountered at lower semi-major axis than that of 1128 Astrid. This reflects into a bimodal distribution of the C values as well, with a more pronounced peak at negative C values (see Fig. 9, panel A). Among the causes that could have produced this situation, i) the original fraction of retrograde rotators produced in the collision could have been higher, ii) the ejection velocity field could have been asymmetrical, with a large fraction of members ejected at lower semi-major axis, and iii) some of the members of the family at higher semi-major axis could have been lost in the 5J:-2A mean-motion resonance. Rather than account for any of these mechanisms, or better an unknown combination of the three, we preferred in this work to use a different approach. Since the most interesting dynamics occurs for values of semi-major axis lower than the family center, we just fitted the distribution of C negative values using Eq. 6. Results of our simulations are shown in Fig. 9, panel B, that displays target function $\psi_{\Delta C}$ values in the (Age, V_{EJ}) plane. As determined from the previous section, we used $K = 0.001$ W/m/K and $\rho_{bulk} = \rho_{surf} = 1300$ kg/m^3. Values of other parameters of the model such as C_{YORP}, δ_{YORP} and $c_{reorient}$ and their description can be found in Bottke et al. (2015).

At 1-sigma level, we obtain $T = 135^{+15}_{-20}$ Myr, and $V_{EJ} = 5^{+17}_{-5}$ m/s. Overall, to within the nominal errors, we confirmed the age estimates of Nesvorný et al. (2015) and Spoto et al. (2015). Independent constraints from Sect. 3 imply that $V_{EJ} < 25$ m/s, in agreement with our results.

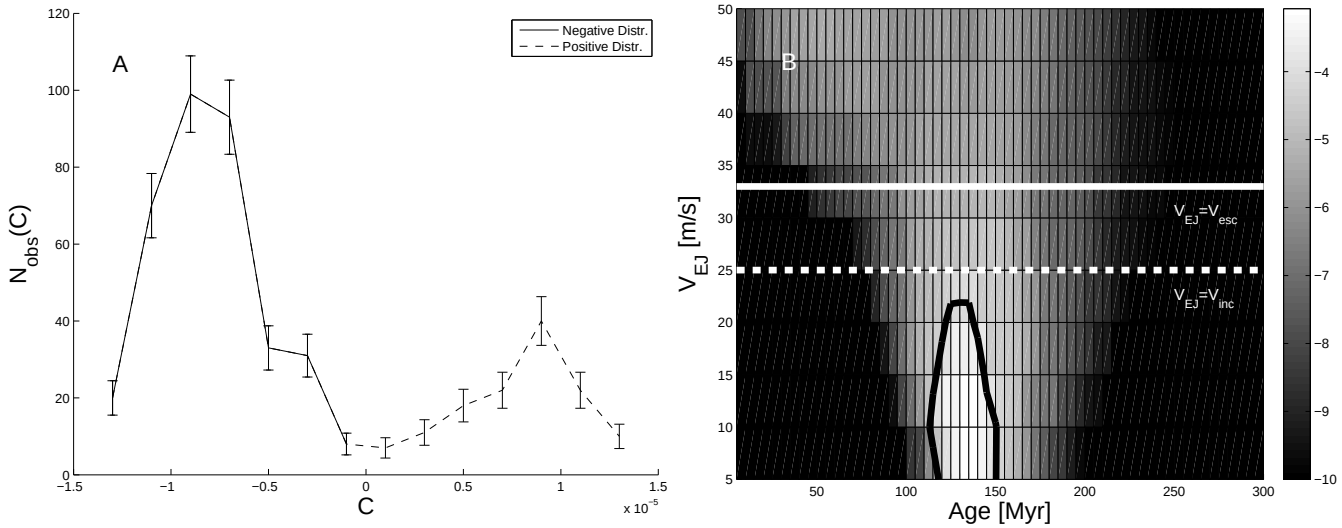

Figure 9. Panel A: Histogram of the distribution of C values for the Astrid family (blue line). The dashed line displays the positive part of the C distribution. Panels B: target function $\psi_{\Delta C}$ values in (Age, V_{EJ}) plane for a symmetrical bimodal distribution based on the C negative values. The horizontal full white line display the value of the estimated escape velocity from the parent body, while the horizontal dashed white line refers to the $V_{EJ} = 25$ m/s limit obtained from the current inclination distribution in Sect. 3. The black thick line displays the contour level of $\psi_{\Delta C}$ associated with a 1-sigma probability that the simulated and real distribution were compatible.

6 CONCLUSIONS

Our results could be summarized as follows:

- We identify the Astrid family in the domain of proper elements, and eliminated albedo and photometric interlopers. The Astrid family is a C-complex family and C-complex objects dominate the local background. 19 members of the family are in $s - s_C$ resonant librating states, and appear to oscillate around the stable point at $\Omega - \Omega_C = \pm 90°$. The width of the librating region of the $s - s_C$ resonance is equal to 0.8 arcsec/yr, and any cluster of objects injected into the resonance would have its members completely dispersed along the separatrix of the $s - s_c$ resonance on timescales of the order of 10 Myr.
- Assuming that the original ejection velocity field of the Astrid family could be approximated as isotropic, the V_{EJ} parameter describing the standard deviation of terminal ejection velocity should not have been higher than 25 m/s, or the family would have been more dispersed in inclination than what currently observed.
- Interaction with the $s - s_C$ increased the value of the kurtosis of the distribution of the v_W component of currently observed ejection velocities to the large value currently observed ($\gamma_2 = 4.43$). Simulations of fictitious Astrid families with standard values of key parameters describing the strength of the Yarkovsky force for C-type asteroids, such as the thermal conductivity $K = 0.01$ W/m/K, fails to produce a distribution of asteroids with $\gamma_2(v_W)$ equal to the current value over the possible lifetime of the family. Constraints from the currently observed number of objects that crossed the $s - s_C$ region, suggest that K could be closer to 0.001 W/m/K for the Astrid members. The bulk and surface density should be higher than 1000 kg/m^3.
- Using a Monte Carlo approach to asteroid family determination (Bottke et al. 2015; Carruba et al. 2015a), and values of thermal conductivity and asteroid mass density obtained from the $\gamma_2(v_W)$ tests, we estimated the Astrid family to be $T = 135^{+15}_{-20}$ Myr old, and its ejection velocity parameter to be in the range $V_{EJ} = 5^{+17}_{-5}$ m/s. In agreement with what found from constraints from the current inclination distribution of family members, values of V_{EJ} larger than 25 m/s were not likely to have occurred.

Overall, the unique nature of the Astrid family, characterized by its interaction with the $s - s_C$ secular resonance and by high values of the γ_2 parameter describing the kurtosis of the v_W component of the currently estimated ejection velocity field allowed for the use of techniques that provided invaluable constraints on the range of permissible values of parameters describing the Yarkovsky force, such as the surface thermal conductivity and density, not available for other asteroid families.

ACKNOWLEDGMENTS

We are grateful to the reviewer of this paper, Prof. Andrea Milani, for comments and suggestions that significantly improved the quality of this paper. We would like to thank the São Paulo State Science Foundation (FAPESP) that supported this work via the grant 14/06762-2, and the Brazilian National Research Council (CNPq, grant 305453/2011-4). This publication makes use of data products from the Wide-field Infrared Survey Explorer (WISE) and NEOWISE, which are a joint project of the University of California, Los Angeles, and the Jet Propulsion Laboratory/California Institute of Technology, funded by the National Aeronautics and Space Administration.

REFERENCES

Beaugé, C., Roig, F., 2001, Icarus, 153, 391.

Bendjoya, P., Zappalà, V. 2002. Asteroids III, W. F. Bottke Jr., A. Cellino, P. Paolicchi, and R. P. Binzel (eds), University of Arizona Press, Tucson, 613.
Bottke, W. F., and 10 co-authors, 2015, Icarus, 247, 191.
Brož, M., 1999. Thesis, Charles Univ., Prague, Czech Republic.
Brož, M., Morbidelli, A., Bottke, W. F., et al. 2013, A&A, 551, A117
Bus, J. S., Binzel, R. P. 2002a. Icarus 158, 106.
Bus, J. S., Binzel, R. P. 2002b, Icarus 158, 146.
Carruba 2009. MNRAS, 395, 358.
Carruba, V. 2010. MNRAS, 408, 580.
Carruba, V., Nesvorný, D., Aljbaae, S., Domingos, R. C., Huaman, M. E., 2015a, MNRAS, 451, 4763.
Carruba, V. Winter, O., Aljbaae, S., 2015b, MNRAS, 455, 2279.
Carruba, V., Nesvorný, D., 2016, MNRAS, 457, 1332.
DeMeo, F., Carry, B., 2013, Icarus, 226, 723.
Ivezić, Ž, and 34 co-authors, 2001, AJ, 122, 2749.
Knežević, Z., Milani, A. (2000), CMDA, 78, 17.
Lazzaro, D., Angeli, C.A., Carvano, J.M., Mothé-Diniz, T., Duffard, R., Florczak, M., 2004, Icarus 172, 179.
Levison, H. F., Duncan, M. J., 1994. Icarus, 108, 18-36.
Masiero, J. R., Mainzer, A. K., Grav, T., Bauer, J. M., and Jedicke, R., 2012, APJ, 759, 14.
Milani, A., Farinella, P., 1994, Nature 370, 40.
Murray, C. D., Dermott, S. F., 1999, Solar System Dynamics, Cambridge Univ. Press, Cambridge.
Nesvorný, D., Brož, M., Carruba, V. 2015, In Asteroid IV, (P. Michel, F. E. DeMeo, W. Bottke Eds.), Univ. Arizona Press and LPI, 297.
Novaković, B., Maurel, C., Tsirvoulis, G., Knežević, Z. 2015, ApJ, 807, L5.
Novakovic, B., Tsirvoulis, G., Maro, S., Djosovic, V., & Maurel, C. 2016, arXiv:1601.00905
Press, V.H., Teukolsky, S. A., Vetterlink, W. T., Flannery, B. P., 2001, Numerical Recipes in Fortran 77, Cambridge Univ. Press, Cambridge.
Russell, C. T., Raymond, C. A., Nathues, A., et al. 2015, IAU General Assembly, 22, #2221738
Spoto, F., Milani, A. Knežević, Z. 2015, Icarus, 257, 275.
Tholen, D. J., 1989, Asteroid Taxonomic Classifications, in Binzel R. P., Gehrels, T., Matthews, M. S. (eds), University of Arizona Press, Tucson, 298.
Vokrouhlický, D. 1999, A&A, 334, 362
Vokrouhlický, D., Brož, M., Morbidelli, A., et al. 2006a, Icarus, 182, 92.
Vokrouhlický D., Brož, M., Bottke, W. F., Nesvorný, D., Morbidelli, A. 2006b, Icarus, 182, 118.
Vokrouhlický D., Brož, M., Bottke, W. F., Nesvorný, D., Morbidelli, A. 2006c, Icarus, 183, 349.

This paper has been typeset from a TEX/LATEX file prepared by the author.